Giant Spin Hall Effect and Switching Induced by Spin-Transfer Torque in a $W/Co_{40}Fe_{40}B_{20}/MgO$ Structure with Perpendicular Magnetic Anisotropy

Qiang Hao and Gang Xiao*

Department of Physics, Brown University, Providence, Rhode Island 02912, USA

(Received 7 November 2014; revised manuscript received 6 February 2015; published 26 March 2015)

We obtain robust perpendicular magnetic anisotropy in a β-$W/Co_{40}Fe_{40}B_{20}/MgO$ structure without the need of any insertion layer between W and $Co_{40}Fe_{40}B_{20}$. This is achieved within a broad range of W thicknesses (3.0–9.0 nm), using a simple fabrication technique. We determine the spin Hall angle (0.40) and spin-diffusion length for the bulk β form of tungsten with a large spin-orbit coupling. As a result of the giant spin Hall effect in β-W and careful magnetic annealing, we significantly reduce the critical current density for the spin-transfer-torque-induced magnetic switching in $Co_{40}Fe_{40}B_{20}$. The elemental β-W is a superior candidate for magnetic memory and spin-logic applications.

DOI: 10.1103/PhysRevApplied.3.034009

I. INTRODUCTION

Recently, the spin Hall effect (SHE) [1–3] has received much attention. Particularly noteworthy is the phenomenon of the giant spin Hall effect (GSHE) [4–13] in nonmagnetic metals with strong spin-orbit coupling (SOC). Very large spin Hall angles (Θ) have been discovered in solids ranging from simple SOC solids of Pt ($|\Theta| = 0.08$) [4–8], Ta (0.15) [9], and W (0.30) [10,11] to topological insulators, Bi_2Se_3 (2.0–3.5) [12] and $BiSbTe_3$ (1.4–4.25) [13]. With a large Θ, a metal can convert efficiently a longitudinal electrical charge current (J_C) to a transverse spin current (J_S), which can be used to manipulate magnetization states in spintronic devices [6,9,14]. GSHE brightens the prospect of magnetic random-access memory (MRAM) and spin-logic devices. One promising embodiment of MRAM is to prepare an interface between a GSHE solid and a ferromagnetic thin film (FM) with perpendicular magnetic anisotropy (PMA), commonly referred to as a free layer. The injected spin current from the GSHE solid yields a spin-transfer torque (STT) inside the free layer to effect magnetization switching [15,16]. The magnetic states representing the digital bits are sensed by an integrated magnetic sensor, e.g., a magnetic tunneling junction [9,17] or a giant magnetoresistive element. The conjectured STT MRAM with PMA has the advantages of low power consumption, high reliability and durability, and data nonvolatility, over earlier generations of MRAM.

Among the limited number of GSHE solids uncovered so far, tungsten in its highly resistive, metastable β phase is fundamentally interesting for its large SOC, and potentially useful in applications. Having the largest spin Hall angle (0.3) among transition metals, its preparation is compatible to modern semiconductor fabrication processes. However, structures of β-W and FM with PMA have not been obtained. Although PMA can be enabled by inserting a Hf layer into the bilayer, as in β-$W/Hf/Co_{40}Fe_{40}B_{20}$ [10], the Hf layer has the deleterious effects of lowering the effective Hall angle and increasing fabrication complexity. Furthermore, β-W itself is not well studied; for example, the intrinsic spin Hall angle and spin-diffusion length in bulk β-W remain undefined.

In this paper, we report the achievement of β-$W/Co_{40}Fe_{40}B_{20}/MgO$ with robust PMA without the need of any insertion layer. We successfully extend the thickness of β-W to 9.0 nm in this structure, which allows us to explore the variation of spin Hall angle over a broad range of β-W thicknesses. As a result, we determine that the bulk-limit spin Hall angle is 0.40 and the spin-diffusion length is 3.5 nm for β-W. Both parameters are key to the understanding of β-W in the context of GSHE, and to the development of STT MRAM and spin logic incorporating β-W and FM with PMA. The STT-induced switching current for magnetization reversal is of the order of 10^6 A/cm^2, 1 order of magnitude smaller than other similar structures [9,10].

II. SAMPLE PREPARATION AND CHARACTERIZATION

We prepare our layered structures (stacks) on thermally oxidized Si wafers using a high-vacuum magnetron sputtering system. The base pressure is less than 2×10^{-8} Torr and the Ar sputtering pressure is ~2.2 mTorr. For each sample, the whole stack is sequentially deposited in the order of $W/Co_{40}Fe_{40}B_{20}/MgO/Ta$. The capping layer, (1.0)Ta with thickness given in nanometers (nm), is used to prevent oxidation of the active layers from atmosphere. The dc sputtering power for $Co_{40}Fe_{40}B_{20}$ is kept at 10 W. The thickness of the $Co_{40}Fe_{40}B_{20}$ layer is always fixed at 1.0 nm, allowing $Co_{40}Fe_{40}B_{20}$ to develop

*Gang_Xiao@Brown.edu

the PMA. For the formation of β-W, we apply a low dc sputtering power of only 3 W intermittently to keep the deposition rate below 0.02 nm/s. Multiple stacks are made with W thickness in the range of the 2.5 to 9.0 nm. These stacks are patterned using photolithography into standard Hall bars for both Hall effect and resistivity measurements, with the longitudinal dimensions of 20×55 μm^2 in area. Finally, the stacks are annealed at 280 °C for 1 min with 2 h of ramping up and 6 h of natural cooling in vacuum (1×10^{-6} Torr) and magnetic field (0.45 T), which is perpendicular to the stacks. We perform magnetotransport measurements on these stacks using an electromagnet at room temperature. We use the Quantum Design Physical Property Measurement System to measure the saturated magnetization (M_s) of the stacks at room temperature. M_s for $(1.0)Co_{40}Fe_{40}B_{20}$ in the stacks is about 1100 emu/cm^3. To confirm the phase of β-W, we measure the sheet resistance ($R_\square$) of the stacks denoted by $(t)W/(1.0)Co_{40}Fe_{40}B_{20}/(1.6)MgO/(1.0)Ta$. Figure 1 shows the value of $R_\square$ as a function of W thickness from 2.5 to 9.0 nm. The solid line is the best fit to the data based on extracted resistivities of $\rho_W \approx 210$ $\mu\Omega$ cm and $\rho_{Co_{40}Fe_{40}B_{20}} \approx 80$ $\mu\Omega$ cm, according to the relationship

$$R_\square = \left(\frac{\rho_W}{t}\frac{\rho_{Co_{40}Fe_{40}B_{20}}}{t_{Co_{40}Fe_{40}B_{20}}}\right) \Big/ \left(\frac{\rho_W}{t} + \frac{\rho_{Co_{40}Fe_{40}B_{20}}}{t_{Co_{40}Fe_{40}B_{20}}}\right). \quad (1)$$

Typical resistivities for the stable α-W phase and the metastable β-W phase are below 40 $\mu\Omega$ cm and above 150 $\mu\Omega$ cm, respectively. The high resistivity that we obtain indicates that we have β-W in all samples presented here.

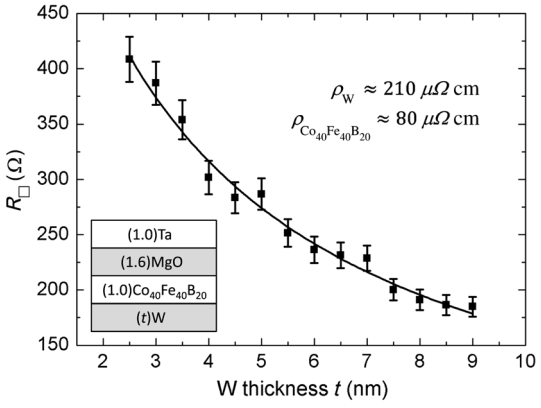

FIG. 1. Sheet resistance ($R_\square$) of $(t)W/(1.0)Co_{40}Fe_{40}B_{20}/(1.6)MgO/(1.0)Ta$ (thickness in nanometers) multilayer stacks as a function of W thickness t (2.5–9.0 nm). The solid line is the best fit to the data based on extracted resistivities of $\rho_W \approx 210$ $\mu\Omega$ cm and $\rho_{Co_{40}Fe_{40}B_{20}} \approx 80$ $\mu\Omega$ cm.

We also use x-ray diffraction to confirm the β-W structure in a film with thickness of 9 nm.

III. RESULTS AND DISCUSSIONS

The conditions for the magnetotransport measurement are illustrated in Fig. 2(a). We send in a direct current along the y axis of a Hall-bar sample, and measure the Hall voltage along the x axis. We apply the external magnetic field ($\mathbf{B}_{ext}$) in the y-z plane with an angle β between the field and y axis. The resulting magnetization vector ($\mathbf{M}$) is also in the y-z plane at an angle θ from the y axis. Figure 2(b) shows the anomalous Hall resistance (R_H) as a function of magnetic field applied perpendicularly to the sample plane ($\beta = 90°$) for a series of samples with varying W thickness (3.0–9.0 nm), $(t)W/(1.0)Co_{40}Fe_{40}B_{20}/(1.6)MgO/(1.0)Ta$. The square hysteresis loops for every sample reveal the attainment of PMA in the $W/Co_{40}Fe_{40}B_{20}$ without the need of an insertion layer between W and $Co_{40}Fe_{40}B_{20}$. The switching field, or coercivity H_c, ranges from 5 to 22 Oe.

The anomalous Hall effect provides a sensing mechanism to measure the magnetization state of the $Co_{40}Fe_{40}B_{20}$ layer. From here on, we investigate how this state responds to an excitation current (I) in the W layer and $\mathbf{B}_{ext}$. Figures 2(c) and 2(d) show current-induced magnetic-switching behavior of a representative sample, $(7.0)W/(1.0)Co_{40}Fe_{40}B_{20}$, under a series of positive ($\beta = 0°$) or negative ($\beta = 180°$) in-plane fields ($B_{ext} = 0.2$, 0.4, 0.7, and 2.0 mT). The bistable states of $\mathbf{M}$ (up and down) are accessible by cycling the current in both directions through a critical value (I_C), under either a positive or negative B_{ext}. We define the critical current (I_C) as the average of the positive and negative switching current. The values of switching current are somewhat different for $\beta = 0°$ and $\beta = 180°$. This difference is due to the hysteretic nucleation process which is stochastic. For $(7.0)W/(1.0)Co_{40}Fe_{40}B_{20}$, $I_C \approx 2.8$ mA for $\beta = 0°$ and 3.4 mA for $\beta = 180°$, yielding an average $I_C \approx 3.1$ mA. Based on $\rho_W \approx 210$ $\mu\Omega$ cm and $\rho_{Co_{40}Fe_{40}B_{20}} \approx 80$ $\mu\Omega$ cm, we estimate that the critical current and the critical current density in the W layer are $I_C(W) \approx 2.3$ mA and $J_C(W) \approx 1.6 \times 10^6$ A/cm^2, respectively, under an in-plane field of 2.0 mT. In this particular sample, the current passing through the W layer is 82.1% of the total current through the stack $(7.0)W/(1.0)Co_{40}Fe_{40}B_{20}$. This critical current density is about 1 order of magnitude smaller than those obtained in other PMA structures: $Ta/Co_{40}Fe_{40}B_{20}$ [9,18,19], Pt/Co [20], and $W/Hf/Co_{40}Fe_{40}B_{20}$ [10].

The current-induced magnetic switching in PMA structures is explained by the spin-transfer torque mechanism due to the injected spin current density (J_S) from the SOC solid with GSHE [20]. Under the measurement conditions of Fig. 2(a), the equilibrium orientation (θ) of $\mathbf{M}$ in the PMA $Co_{40}Fe_{40}B_{20}$ layer is determined from the condition that the net torque on $\mathbf{M}$ is zero [20], i.e.,

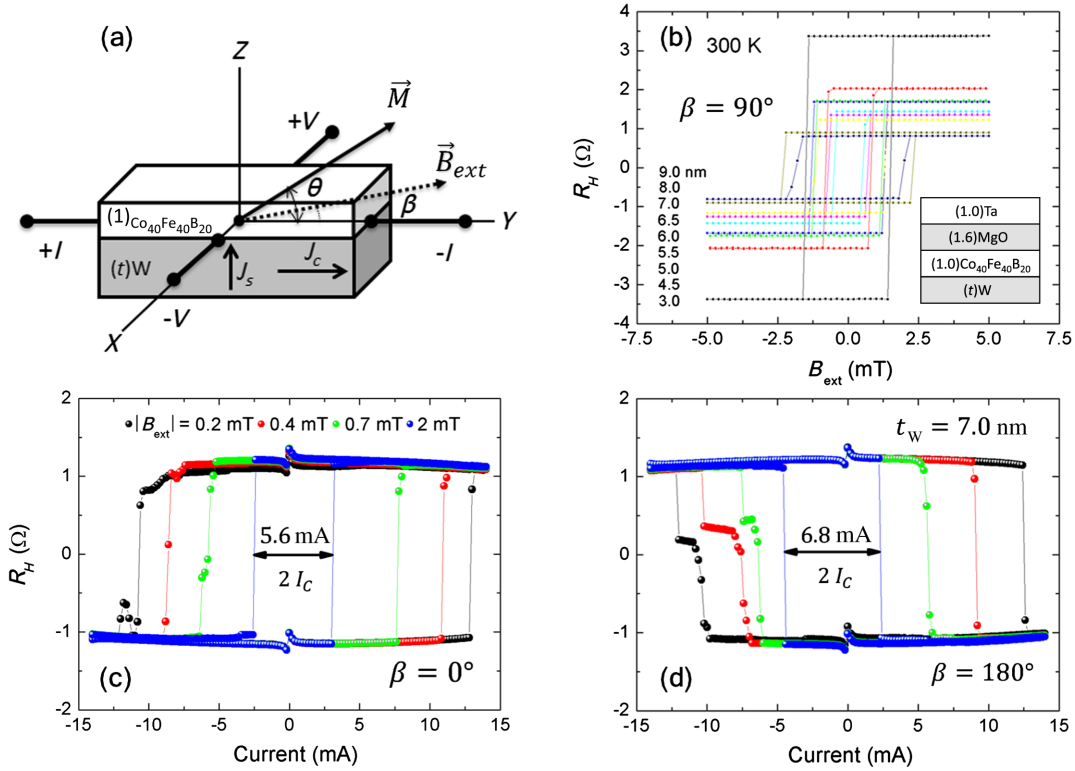

FIG. 2. (a) A schematic of $W/Co_{40}Fe_{40}B_{20}$ bilayer in the Hall-bar configuration for magnetotransport measurement under an external magnetic field ($\mathbf{B}_{ext}$) and an excitation dc current (I). J_C is the charge current density in the W layer, and J_S is the SHE converted spin current density into the $Co_{40}Fe_{40}B_{20}$ layer. (b) Anomalous Hall resistance versus cycling external magnetic field applied perpendicularly to the stacks of $(t)W/(1.0)Co_{40}Fe_{40}B_{20}/(1.6)MgO/(1.0)Ta$ (t: 3.0–9.0 nm). (c),(d) Current-induced magnetic-switching curves in the $(7.0)W/(1.0)Co_{40}Fe_{40}B_{20}/(1.6)MgO/(1.0)Ta$ sample, under either a positive ($\beta = 0°$) (c) or a negative ($\beta = 180°$) (d) external field B_{ext} (0.2, 0.4, 0.7, 2.0 mT). From each switching curve, critical current (I_C) can be obtained as shown.

$$\begin{aligned}\tau_{tot} &\equiv \hat{x}\cdot(\vec{\tau}_{ST}+\vec{\tau}_{ext}+\vec{\tau}_{an})\\ &= \tau^0_{ST}+B_{ext}\sin(\theta-\beta)-B^0_{an}\sin\theta\cos\theta\\ &= 0,\end{aligned} \tag{2}$$

where $\tau^0_{ST}=(\hbar/2eM_st)J_S$ is the torque per unit moment, and B^0_{an} is the perpendicular anisotropy field. This macrospin model predicts the current-induced magnetic switching, as shown in Figs. 2(c) and 2(d), at sufficient current density ($>J_C$) or corresponding spin-transfer torque τ^0_{ST} per unit moment.

In the coherent spin-rotation regime, Eq. (2) is also used as a method to measure τ^0_{ST}, hence, the converted spin current density J_S from which the spin Hall angle can be derived ($\Theta = J_S/J_C$) [20]. In Eq. (2), the angle (θ) can be obtained from the anomalous Hall resistance, $R_H/R_0=\sin\theta$, where R_0 is the maximum Hall resistance when $\mathbf{M}$ is perpendicular to the sample plane. According to Eq. (2), as B_{ext} approaches zero or infinity, θ reaches 0° or 90°, respectively. Under an intermediate B_{ext}, θ is dependent on τ^0_{ST}, B_{ext}, and B^0_{an}, as demonstrated in Fig. 3(a), which shows how the R_H or $\sin\theta$ varies as a function of B_{ext} under a positive or a negative current of 2 mA. It can be seen in Fig. 3(a) that, at an arbitrary $\sin\theta$, there exist two B_{ext} values, $B_+(\theta)$ and $B_-(\theta)$, corresponding to the positive and negative current, respectively. From Eq. (2),

$$\tau^0_{ST}(+J_S)+B_+(\theta)\sin(\theta-\beta)-B^0_{an}\sin\theta\cos\theta=0, \tag{3}$$

$$\tau^0_{ST}(-J_S)+B_-(\theta)\sin(\theta-\beta)-B^0_{an}\sin\theta\cos\theta=0. \tag{4}$$

By solving the simultaneous equations using a combination of Eq. (3)±Eq. (4), one obtains,

$$[B_+(\theta)-B_-(\theta)]=-\Delta\tau^0_{ST}/\sin(\theta-\beta), \tag{5}$$

$$[B_+(\theta)+B_-(\theta)]=2B^0_{an}\sin\theta\cos\theta/\sin(\theta-\beta), \tag{6}$$

where $\Delta\tau^0_{ST}=\tau^0_{ST}(+J_S)-\tau^0_{ST}(-J_S)=2\tau^0_{ST}(|J_S|)$. The experimental procedure implied in Fig. 3(a) generates the quantities of $B_+(\theta)$, $B_-(\theta)$, and θ. Then, using Eqs. (5) and (6), one can calculate $\tau^0_{ST}(|J_S|)$ and B^0_{an}. Figure 3(b) shows $[B_+(\theta)-B_-(\theta)]$ as a function of $1/\sin(\theta-\beta)$, based on the data in Fig. 3(a). As predicted by Eq. (5), linear relations are confirmed for various current values, and the slope is $\Delta\tau^0_{ST}$ for each supplied current.

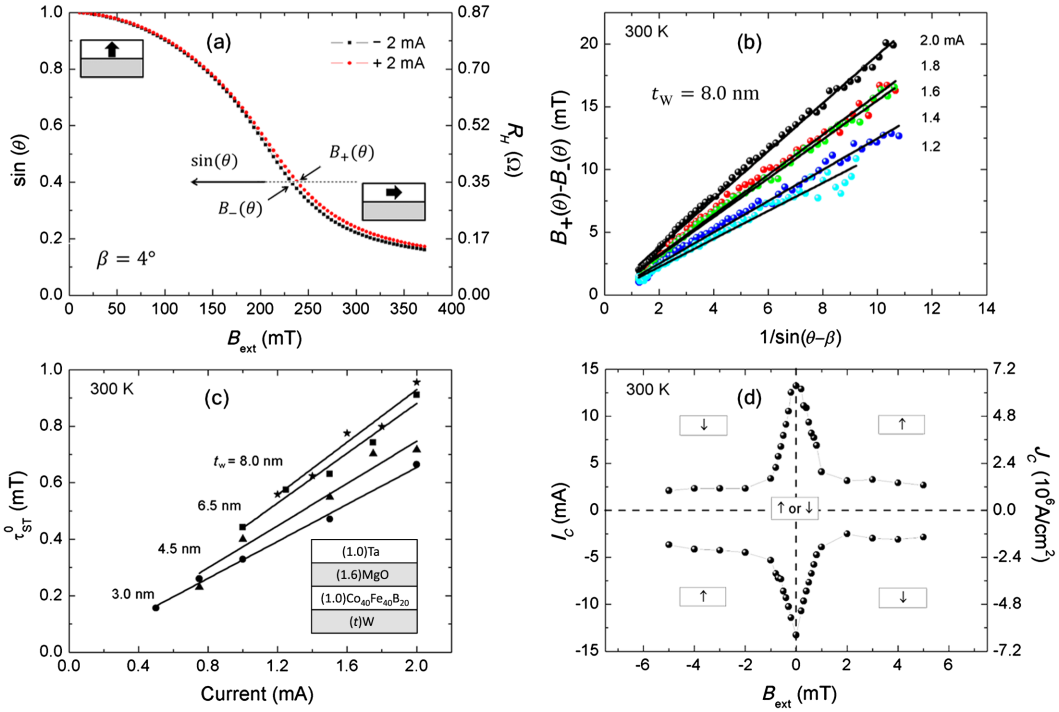

FIG. 3. (a) Normalized Hall resistance (i.e., $\sin\theta$) as functions of nearly in-plane magnetic field B_{ext} ($\beta = 4°$) under a positive or negative current (± 2 mA). θ is the angle between the magnetization vector $\mathbf{M}$ and the y axis. $B_+(\theta)$ and $B_-(\theta)$ are the magnetic fields required to rotate the $\mathbf{M}$ to θ corresponding to the positive and the negative current, respectively. (b) Linear relationships between $B_+(\theta) - B_-(\theta)$ and $1/\sin(\theta - \beta)$ under different excitation current (0.5–2 mA). The slope for each fitted straight line is the net spin-transfer torque per unit moment, $\Delta\tau^0_{\text{ST}}$, between the positive and negative excitation current. (c) Spin-transfer torques (τ^0_{ST}) per unit moment as functions of excitation currents for (t)W/(1.0)$Co_{40}Fe_{40}B_{20}$/(1.6)MgO/(1.0)Ta (t: 3.0–9.0 nm). All the torques are linear in current and vanish as current approaches zero. Thicker W generates more torque per unit of current. (d) Magnetic-switching phase diagram of (7.0)W/(1.0)$Co_{40}Fe_{40}B_{20}$/(1.6)MgO/(1.0)Ta, in the parameter space of B_{ext} and critical current (I_C) or critical current density (J_C). The arrows (↑ or ↓) denote the directions of the $\mathbf{M}$ vector in various regions. I_C is the net current into the Hall bar, and J_C is the corresponding current density *only* in the W layer. The lines connecting the data are guides to the eyes.

Using this method, we determine the spin-transfer torque per unit moment $\tau^0_{\text{ST}}(|J_S|)$ versus current in our samples with varying W thickness, as shown in Fig. 3(c). We also determine that the anisotropy field B^0_{an} is 214 mT for the sample used in Fig. 3(b).

Based on data in Fig. 3(c), we calculate the spin Hall angle according to $\Theta = J_S/J_C = (2eM_s t/\hbar)(\tau^0_{\text{ST}}/J_C)$. Figure 4 shows the spin Hall angle as a function of W thickness (t) from 3.0 to 9.0 nm for the (t)W/(1.0)$Co_{40}Fe_{40}B_{20}$/(1.6)MgO/(1.0)Ta system with PMA. At 9.0 nm, the spin Hall angle is 0.35 ± 0.04. In the thinner limit, the spin Hall angle decreases, as the W thickness becomes comparable to the spin-diffusion length (λ_{sf}). The variation of the Hall angle versus W thickness allows us to obtain $\Theta(\infty) = 0.40 \pm 0.03$ and $\lambda_{sf} = 3.5 \pm 0.3$ nm in the bulk β-W film, according to $[J_S(t)/J_S(\infty)] = [\Theta(t)/\Theta(\infty)] = 1 - \text{sech}(t/\lambda_{sf})$ [21], which is used to fit the data in Fig. 4. In comparison, $\Theta(5.2\,\text{nm}) = 0.33 \pm 0.06$ is obtained in $W/Co_{40}Fe_{40}B_{20}/MgO$ with in-plane

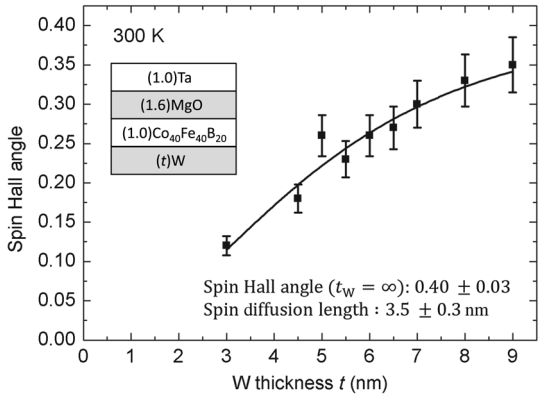

FIG. 4. Spin Hall angles versus W thickness for (t)W/(1.0)$Co_{40}Fe_{40}B_{20}$/(1.6)MgO/(1.0)Ta (t: 3.0–9.0 nm). The line represents theoretical fitting to the data assuming a finite spin-diffusion length in the β-W film. For the bulk β-W film, spin Hall angle is determined to be 0.40 ± 0.03 and spin-diffusion length is 3.5 ± 0.3 nm at room temperature.

magnetic anisotropy [11], and *effective* $\Theta(4\ \mathrm{nm}) = 0.34 \pm 0.05$ in $W/Hf/Co_{40}Fe_{40}B_{20}/MgO$ with Hf-induced PMA [10]. Our determination of the bulk $\Theta(\infty)$ and λ_{sf} for β-W is beneficial to further theoretical understanding of this important SOC solid and to the design of spintronic devices by selecting appropriate β-W thickness. Moreover, PMA can be achieved in $W/Co_{40}Fe_{40}B_{20}/MgO$ without the need of any insertion layer which reduces spin Hall angle [10].

As shown earlier in Fig. 2(c), with sufficient current (i.e., spin-transfer torque), **M** of the $Co_{40}Fe_{40}B_{20}$ layer will undergo switching, which can also be described by Eq. (2). Based on results in Fig. 2(c), we obtain the magnetic-switching phase diagram, shown in Fig. 3(d), for a representative sample $(7.0)W/(1.0)Co_{40}Fe_{40}B_{20}/(1.6)MgO$ (area $20 \times 55\ \mu m^2$). The critical switching current density (J_C) in the W layer decreases rapidly and linearly with increasing field (B_{ext}) up to a characteristic field $B_0 \sim 1$ mT, and at a slower rate when $B_{\mathrm{ext}} > B_0$. As a comparison, $B_0 \sim 15$ mT and 300 mT are measured for two other PMA systems, $(5.0)Ta/(0.6\ \mathrm{nm})CoFe/(1.8)MgO$ (area $1.2 \times 15 \mu m^2$) [22] and $(2.0)Pt/(0.6)Co/AlO_x$ ($20 \times 200\ \mu m^2$) [20], respectively. The significantly lower B_0 obtained in our PMA system bodes well for achieving reliable switching under a small external field. In STT MRAM or spin-logic applications, a low biasing field can be much more easily implemented than a 10-times larger field. It is noted that B_0 is of the magnitude of the nucleation field in our system [see coercivity values in Fig. 2(b)]. From Fig. 3(c), we obtain the lowest $J_C \sim 1.6 \times 10^6\ \mathrm{A/cm^2}$ at 2 mT, about 5 to 10 times smaller than other PMA systems [9,10,18–20]. Our insight is that the observed low critical current density is partly due to the GSHE, and partly to the low coercivity in our samples, which we developed through meticulous optimization of magnetic thermal annealing.

IV. CONCLUSIONS

We observe GSHE in a β-$W/Co_{40}Fe_{40}B_{20}/MgO$ system with perpendicular magnetic anisotropy. We determine that the spin Hall angle is 0.40 ± 0.03 and spin-diffusion length is 3.5 ± 0.3 nm in bulk β-W film at room temperature. It is the largest spin Hall angle among elemental solids with a large spin-orbit coupling [4–11,23,24]. We obtain the magnetic-switching phase diagram of the PMA $Co_{40}Fe_{40}B_{20}$ driven by spin-transfer torque from the β-W. Under an in-plane biasing field of only 2 mT, the switching current density is about $1.6 \times 10^6\ \mathrm{A/cm^2}$, which is the lowest among other PMA systems with GSHE. We demonstrate that, without the need of any tricks such as the use of insertion layer, thick β-W films can be integrated with the well-known $Co_{40}Fe_{40}B_{20}$ ferromagnetic film to achieve a robust PMA. The large Hall angle and acquired PMA makes β-W an ideal candidate for STT MRAM and spin-logic applications, with the added advantage of its compatibility with modern semiconductor fabrication. We also note that the long spin-diffusion length would require somewhat thicker β-W film to take full advantage of its GSHE. A thicker film tends to increase the total current, which, coupled with the high resistivity of the β-W film, may require more power for magnetic switching.

ACKNOWLEDGMENTS

We wish to thank Wenzhe Chen and Shu-tong Wang for assistance and discussion. This work was supported by Nanoelectronics Research Initiative (NRI) through the Institute for Nanoelectronics Discovery and Exploration (INDEX) and by National Science Foundation through Grants No. DMR-1307056 and No. DMR-1229195.

[1] M. I. Dyakonov and V. I. Perel, Current-induced spin orientation of electrons in semiconductors, Phys. Lett. **35A**, 459 (1971).
[2] J. E. Hirsch, Spin Hall Effect, Phys. Rev. Lett. **83**, 1834 (1999).
[3] S. Zhang, Spin Hall Effect in the Presence of Spin Diffusion, Phys. Rev. Lett. **85**, 393 (2000).
[4] A. Azevedo, L. H. Vilela-Leão, R. L. Rodríguez-Suárez, A. F. Lacerda Santos, and S. M. Rezende, Spin pumping and anisotropic magnetoresistance voltages in magnetic bilayers: Theory and experiment, Phys. Rev. B **83**, 144402 (2011).
[5] N. Vlietstra, J. Shan, V. Castel, J. Ben Youssef, G. E. W. Bauer, and B. J. van Wees, Exchange magnetic field torques in YIG/Pt bilayers observed by the spin-Hall magnetoresistance, Appl. Phys. Lett. **103**, 032401 (2013).
[6] L. Liu, T. Moriyama, D. C. Ralph, and R. A. Buhrman, Spin-Torque Ferromagnetic Resonance Induced by the Spin Hall Effect, Phys. Rev. Lett. **106**, 036601 (2011).
[7] O. J. Lee, L. Q. Liu, C. F. Pai, Y. Li, H. W. Tseng, P. G. Gowtham, J. P. Park, D. C. Ralph, and R. A. Buhrman, Central role of domain wall depinning for perpendicular magnetization switching driven by spin torque from the spin Hall effect, Phys. Rev. B **89**, 024418 (2014).
[8] A. Ganguly, K. Kondou, H. Sukegawa, S. Mitani, S. Kasai, Y. Niimi, Y. Otani, and A. Barman, Thickness dependence of spin torque ferromagnetic resonance in $Co_{75}Fe_{25}/Pt$ bilayer films, Appl. Phys. Lett. **104**, 072405 (2014).
[9] L. Liu, C.-F. Pai, Y. Li, H. W. Tseng, D. C. Ralph, and R. A. Buhrman, Spin-torque switching with the giant spin Hall effect of tantalum, Science **336**, 555 (2012).
[10] C.-F. Pai, M.-H. Nguyen, C. Belvin, L. H. Vilela-Leão, D. C. Ralph, and R. A. Buhrman, Enhancement of perpendicular magnetic anisotropy and transmission of spin-Hall-effect-induced spin currents by a Hf spacer layer in W/Hf/CoFeB/MgO layer structures, Appl. Phys. Lett. **104**, 082407 (2014).
[11] C.-F. Pai, L. Liu, Y. Li, H. W. Tseng, D. C. Ralph, and R. A. Buhrman, Spin transfer torque devices utilizing the giant spin Hall effect of tungsten, Appl. Phys. Lett. **101**, 122404 (2012).

[12] A. R. Mellnik, J. S. Lee, A. Richardella, J. L. Grab, P. J. Mintun, M. H. Fischer, A. Vaezi, A. Manchon, E.-A. Kim, N. Samarth, and D. C. Ralph, Spin-transfer torque generated by a topological insulator, Nature (London) **511**, 449 (2014).

[13] Y. Fan, P. Upadhyaya, X. Kou, M. Lang, S. Takei, Z. Wang, J. Tang, L. He, L.-T. Chang, M. Montazeri, G. Yu, W. Jiang, T. Nie, R. N. Schwartz, Y. Tserkovnyak, and K. L. Wang, Magnetization switching through giant spin-orbit torque in a magnetically doped topological insulator heterostructures, Nat. Mater. **13**, 699 (2014).

[14] D. Bhowmik, L. You, and S. Salahuddin, Spin Hall effect clocking of nanomagnetic logic without a magnetic field, Nat. Nanotechnol. **9**, 59 (2014).

[15] J. C. Slonczewski, Current-driven excitation of magnetic multilayers, J. Magn. Magn. Mater. **159**, L1 (1996).

[16] J. A. Katine, F. J. Albert, and R. A. Buhrman, Current-induced realignment of magnetic domains in nanostructured Cu/Co multilayer pillars, Appl. Phys. Lett. **76**, 354 (2000).

[17] M. Cubukcu, O. Boulle, M. Drouard, K. Garello, C. O. Avci, I. M. Miron, J. Langer, B. Ocker, P. Gambardella, and G. Gaudin, Spin-orbit torque magnetization switching of a three-terminal perpendicular magnetic tunnel junction, Appl. Phys. Lett., **104**, 042406 (2014).

[18] C. Zhang, M. Yamanouchi, H. Sato, S. Fukami, S. Ikeda, F. Matsukura, and H. Ohno, Magnetization reversal induced by in-plane current in Ta/CoFeB/MgO structures with perpendicular magnetic easy axis, J. Appl. Phys. **115**, 17C714 (2014).

[19] X. Qiu, P. Deorani, K. Narayanapillai, K.-S. Lee, K.-J. Lee, H.-W. Lee, and H. Yang, Angular and temperature dependence of current induced spin-orbit effective fields in Ta/CoFeB/MgO nanowires, Sci. Rep. **4**, 4491 (2014).

[20] L. Liu, O. J. Lee, T. J. Gudmundsen, D. C. Ralph, and R. A. Buhrman, Current-Induced Switching of Perpendicularly Magnetized Magnetic Layers Using Spin Torque from the Spin Hall Effect, Phys. Rev. Lett. **109**, 096602 (2012).

[21] L. Liu, T. Moriyama, D. C. Ralph, and R. A. Buhrman, Spin-Torque Ferromagnetic Resonance Induced by the Spin Hall Effect, Phys. Rev. Lett. **106**, 036601 (2011).

[22] N. Perez, E. Martinez, L. Torres, S.-H. Woo, S. Emori, and G. S. D. Beach, Chiral magnetization textures stabilized by the Dzyaloshinskii-Moriya interaction during spin-orbit torque switching, Appl. Phys. Lett. **104**, 092403 (2014).

[23] H. J. Zhang, S. Yamamoto, Y. Fukaya, M. Maekawa, H. Li, A. Kawasuso, T. Seki, E. Saitoh, and K. Takanashi, Current-induced spin polarization on metal surfaces probed by spin-polarized positron beam, Sci. Rep. **4**, 4844 (2014).

[24] H. L. Wang, C. H. Du, Y. Pu, R. Adur, P. C. Hammel, and F. Y. Yang, Scaling of Spin Hall Angle in 3*d*, 4*d*, and 5*d* Metals from $Y_3Fe_5O_{12}$/Metal Spin Pumping, Phys. Rev. Lett. **112**, 197201 (2014).